

Revealing the structure-property relationships of copper alloys with FAGC

Yuexing Han^{a,b,*}, Guanxin Wan^a, Tao Han^c, Bing Wang^{a,*} and Yi Liu^{c,*}

^aSchool of Computer Engineering and Science, Shanghai University, 99 Shangda Road, Shanghai 200444, People's Republic of China

^bKey Laboratory of Silicate Cultural Relics Conservation (Shanghai University), Ministry of Education

^cMaterials Genome Institute, Shanghai University, Shanghai 200444, People's Republic of China

ARTICLE INFO

Keywords:

Feature Augmentation on Geodesic Curves
Cu-Cr-Zr alloy
Shape space theory
Feature augmentation
Deep learning

ABSTRACT

Understanding how the structure of materials affects their properties is a cornerstone of materials science and engineering. However, traditional methods have struggled to accurately describe the quantitative structure-property relationships for complex structures. In our study, we bridge this gap by leveraging machine learning to analyze images of materials' microstructures, thus offering a novel way to understand and predict the properties of materials based on their microstructures. We introduce a method known as FAGC (Feature Augmentation on Geodesic Curves), specifically demonstrated for Cu-Cr-Zr alloys. This approach utilizes machine learning to examine the shapes within images of the alloys' microstructures and predict their mechanical and electronic properties. This generative FAGC approach can effectively expand the relatively small training datasets due to the limited availability of materials images labeled with quantitative properties. The process begins with extracting features from the images using neural networks. These features are then mapped onto the Pre-shape space to construct the Geodesic curves. Along these curves, new features are generated, effectively increasing the dataset. Moreover, we design a pseudo-labeling mechanism for these newly generated features to further enhance the training dataset. Our FAGC method has shown remarkable results, significantly improving the accuracy of predicting the electronic conductivity and hardness of Cu-Cr-Zr alloys, with R^2 values of 0.978 and 0.998, respectively. These outcomes underscore the potential of FAGC to address the challenge of limited image data in materials science, providing a powerful tool for establishing detailed and quantitative relationships between complex microstructures and material properties.

1. Introduction

Cu-Cr-Zr alloy, as an outstanding high-strength and high conductive copper-based material, plays a crucial role in critical technological fields such as nuclear fusion due to its excellent performance in high-temperature and high-radiation environments. Widely applied in aerospace to nuclear energy industries, its unique properties make it the preferred material for many advanced engineering applications. Particularly in extreme conditions, such as high temperatures, high radiation, and complex mechanical loading, Cu-Cr-Zr alloy exhibits remarkable mechanical and thermal stability, making it indispensable in high-end manufacturing. However, significant challenges persist in the field of materials science, especially in predicting its key properties like electrical conductivity and hardness. Electrical conductivity and hardness are crucial indicators for evaluating the performance of materials in engineering applications, directly impacting their service life and reliability. Moreover, predicting the characteristics of Cu-Cr-Zr alloy is a complex task, influenced by numerous factors, including the specific composition of alloy, temperature, and pressure conditions during processing, as well as the forces and thermal environments experienced in practical applications. The interactions between these factors and the intricate relationships determining the final material performance impose a great challenge. For instance, minute variations in the trace elements of the alloy can significantly affect its

hardness and electrical conductivity. Similarly, processing conditions such as heat treatment temperature and time can alter the microstructure of alloy, influencing its electrical conductivity and hardness. Due to the subtle interplay of alloy composition, processing conditions, and complex thermal and mechanical interactions, predicting these properties becomes daunting. While significant progress has been made in understanding the fundamental properties of Cu-Cr-Zr alloy, there is still a significant gap in current research efforts to predict the electrical conductivity and hardness of these alloys accurately. To bridge the gap, this study proposes a novel machine learning approach to predict the electrical conductivity and hardness of Cu-Cr-Zr alloy precisely based on their microstructures.

In recent years, with the rapid development of machine learning methods [1], there is a growing tendency to design machine learning models to solve engineering problems based on data analysis. Particularly in materials science area, the machine learning methods show great potential by avoiding the necessity for a detailed understanding of physical mechanisms or experimental measurements. Support vector regression (SVR) is a simple and reliable model for nonlinear regression analysis [2–4]. Decision tree regression (DecisionTree) is another traditional machine learning method to suitably solve nonlinear regression problems [5]. For example, a machine learning method based on SVR is employed to predict the distribution of the elastic strain field in high-contrast 3D composites [6]. A highly accurate prediction of the material removal rate for chemical

*Corresponding author.

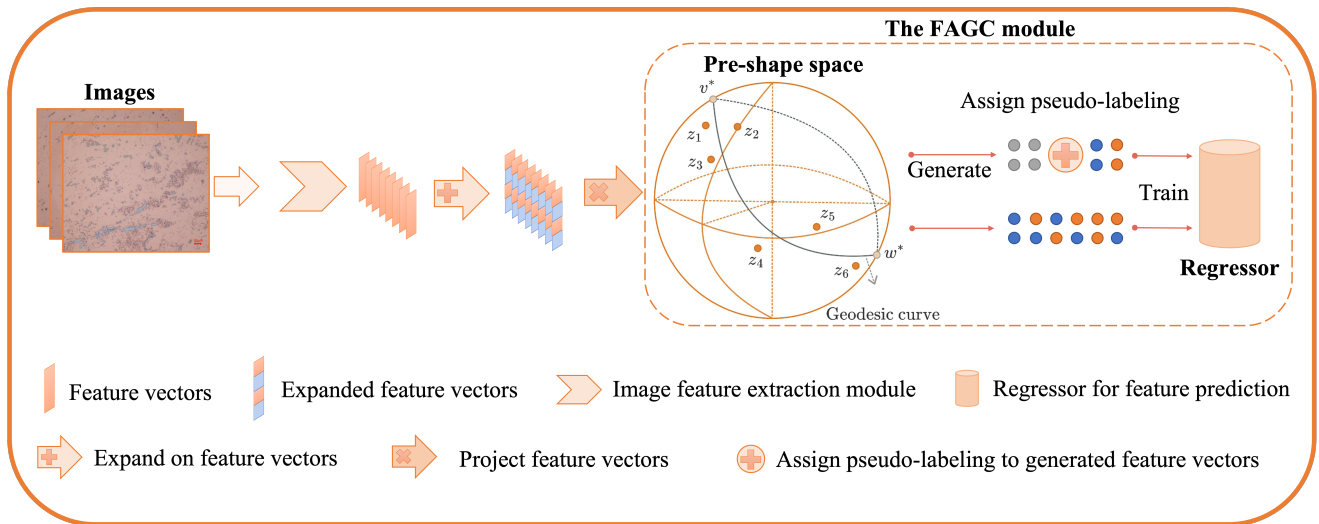


Figure 1: An overview of performance prediction for electrical conductivity and hardness of Cu-Cr-Zr based on Geodesic curve feature augmentation.

mechanical planarization can be achieved using the integrated DecisionTree [7]. However, these traditional machine learning methods still face certain challenges, including difficulties in handling complex relationships between materials and performance, and limitations in extracting more information from images. These shortcomings underscore the demand for more powerful models. With the success of deep learning methods in areas such as image recognition and target recognition[8–11]. The structure and depth of neural networks have also been improved and increased, such as LeNet-5[11], AlexNet[12], ResNet[13], EfficientNet [14], and so on. Moreover, there are still few studies on the image processing of quantitative relationships between structure and properties of materials.

Neural networks have achieved excellent prediction performance on various material images due to their excellent data representation abilities. For example, Han et al. utilized deep learning and digital image processing techniques to statistically analyze the precipitates, especially the size of the sigma phase, in SEM images of 2205 duplex stainless steel (DSS) [15]. They reasonably estimated the average interfacial energy between the s phase and the g phase. The effective thermal conductivity of sintered silver is predicted with superior performance by convolutional neural networks (CNN) compared to that achieved by conventional machine learning regression models [16]. Similarly, a model with an enhanced CNN structure to predict the effective thermal conductivity of composites and porous media[17]. The network model demonstrated strong performance on 1500 composite datasets generated by a quadratic structure generating set [18]. However, the performance of these convolutional neural networks heavily depends on the training dataset size. It is difficult to achieve satisfactory performance using raw images directly as input to the neural network model for small datasets or specific materials microscopic images. Therefore, it is necessary to increase the dataset

size using data augmentation techniques to improve the prediction accuracy and generalization ability of the model.

There are three main types of data augmentation methods. The first one is to add some perturbing factors to the image, such as panning, rotating, cropping, adding noise, and other image processing methods [19]. The perturbation method is often ineffective, and loses critical information. The second type of data augmentation is generative models, which produce new data by learning from real data, such as GAN [20] and VAE[21]. These models are widely used in the field of data augmentation because of their excellent generative abilities. However, the generative models rely too much on a large amount of training data. These models generate poor quality images for the small datasets, such as our Cu-Cr-Zr image dataset. The third type of data augmentation method is to augment the features extracted from the data, i.e., feature augmentation. For feature augmentation enhances the representational ability of data by adapting and changing the features. Feature augmentation does not depend on the data type. One of the primary coping strategies is the transformation of the feature space. For instance, the stochastic feature-enhanced SFA algorithm leverages class-conditional covariance matrix information during neural network training to enhance model performance [22]. Furthermore, Li et al. introduced a technique termed moment exchange for implicit feature enhancement [23]. This method encourages the utilization of moment information from potential features at one instance to replace current moment information, thereby enhancing features. It can effectively reduce the computational complexity and improve data characterization by projecting the data in feature space into another space, such as the Pre-shape space.

The shape space and the Pre-shape space, as two manifold spaces, is first proposed by Kendall to describe an object and all its equivalent variations in a non-Euclidean space [24]. In the shape space, the position, scale, and

orientation of a shape are negligible. Therefore, the shape space theory can be used for object recognition scenarios [25, 26]. Compared to the Euclidean space, the vector in the Shape space captures the intrinsic geometric structure of the data sufficiently. In addition, the shape space theory is not sensitive to the size of the dataset. In the shape space and the Pre-shape space, the Geodesic distance is used to measure the similarity between two shapes. A Geodesic curve can be constructed to fit two orthogonal vectors in a Pre-Shape space [27, 28], Furthermore, Ref. [29] proposed the methods for the non-orthogonal vectors to construct a Geodesic curve. Then, the new data can be produced from the structured Geodesic curves, i.e., data augmentation [26, 29]. Han et al. proposed a method of the feature augmentation on Geodesic curve (FAGC) of which a Geodesic curve is constructed for some vectors in the Pre-Shape space.

Here, we propose prediction method for the mechanical and electronic properties of Cu-Cr-Zr alloys based on FAGC. First, the Cu-Cr-Zr image features are extracted by EfficientNet-B6 [14] and these features as vectors are projected into a Pre-shape space. Some Geodesic curves are constructed to fit these feature vectors. The new feature vectors are generated on the Geodesic curves. Moreover, a pseudo-labeling mechanism is designed for the generated features to expand the feature-property dataset of Cu-Cr-Zr. The performance of the regression model for Cu-Cr-Zr is significantly improved by learning the expanded dataset after feature augmentation. Figure 1 briefly summarizes the framework of Cu-Cr-Zr performance prediction. In summary, our key contributions can be outlined as follows:

- The mechanical and electronic properties of Cu-Cr-Zr alloys are predicted utilizing the FAGC module.
- A pseudo-labeling mechanism has been ingeniously devised for the generated features of Geodesic curves. The pseudo-labeling mechanism expands the dataset size and improves the prediction accuracy and generalization ability of the regression model.

2. Methods

2.1. Feature extraction with EfficientNet-B6

Before applying the feature augmentation with the FAGC module, we extract the features from the input Cu-Cr-Zr images. Most neural network models can extract the discriminative features, which improve the generalization ability of the model for proposing the data of Cu-Cr-Zr. Here, EfficientNet-B6[14] is chosen as the feature extractor and fine-tuned to fit our dataset. Because EfficientNet skillfully balances depth, width, and resolution through a unified scaling coefficient, it achieves superior image recognition performance while optimizing computational efficiency. As shown in Figure 2, the architecture of EfficientNet-B6 consists of an input layer (i.e., material image), an output layer (i.e., material properties), and multiple convolutional layers. The image features are extracted from these the convolutional layers with the neural kernels, which is a

matrix of a specific size. The role of the pooling layer is to reduce the amount of calculation and the number of parameters by reducing the spatial dimension of the feature map. Through the combination of multiple convolutional and pooling layers, various features can be gradually extracted and represented at a fixed size in the feature map. Then, the fully connected layer is employed to convert the final feature map into a one-dimensional vector.

Moreover, unlike other conventional convolutional neural network models, the exceptional performance of EfficientNet is attributed to its core network building block, i.e., the Mobile Inverted Bottleneck Convolution (MBConv) [30], as depicted in Figure 3. First, the technique of expansion convolution with a 1×1 convolution kernel is introduced into the MBConv block to expand the depth of the feature map. While preserving the original spatial resolution, the feature dimension is increased with the MBConv block. Thus, the representational ability of the EfficientNet-B6 is enhanced by the MBConv block to enable a more comprehensive capture of complex structures. Next, the MBConv block also employs depthwise separable convolution[31], which consists of two key stages. The first stage is deep convolution, where spatial filters are applied individually to each channel. This approach minimizes calculation complexity by processing each channel separately instead of processing the combined features of all channels. Second, the MBConv block combines the independent channel information using a 1×1 convolution kernel, which not only recovers the depth of the feature map but also merges the information from the different channels. To enhance the nonlinear properties of the network, the activation function Swish [32] is chosen, which is a nonlinear and smooth to help the network learn more complex feature representations:

$$\text{swish}(x) = x\sigma(\beta x), \quad (1)$$

where $\sigma(\cdot)$ is a logistic function and β is a learnable parameter or a defined hyperparameter. The $\sigma(\cdot) \in (0, 1)$ can be seen as a soft gating mechanism. If $\sigma(\beta x)$ is close to 1, the output of the activation function approximates x . In contrast, if $\sigma(\beta x)$ is close to 0, the output of the activation function approximates 0.

In addition, the original EfficientNet-B6 model is a multi-class classifier, which does not directly applicable to the current task. Therefore, the output of the fully connected layers of the EfficientNet-B6 are adjusted to be compatible with the Cu-Cr-Zr image data. These modifications are crucial for the output image performance metrics. Meanwhile, the EfficientNet-B6 model has been pre-trained on the widely used ImageNet dataset[8], which contains about 1.2 million images. The training process for the feature extractor employs the mean square error as the loss function, continuing until the loss value stabilizes. This stabilization indicates that the model has effectively learned and adapted to the training data. Then, the output data of the EfficientNet-B6 network is selected as the extracted feature data for the subsequent expansion of the features.

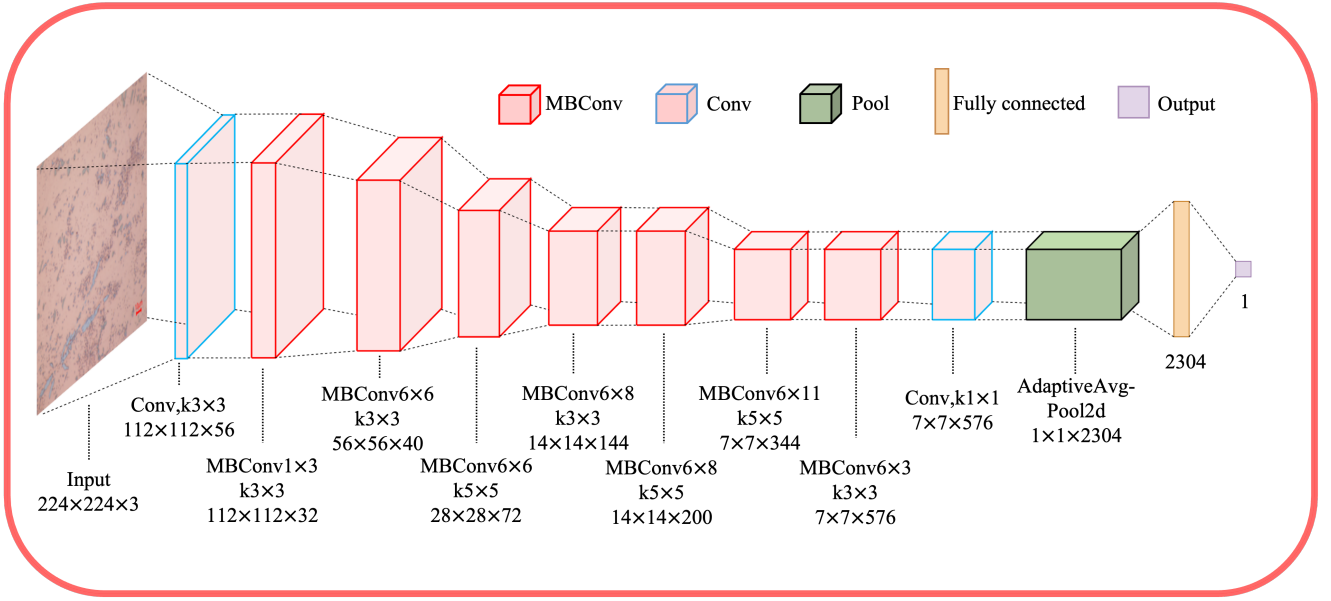


Figure 2: The network architecture of EfficientNet-B6 using MBConv6 as a fundamental building block.

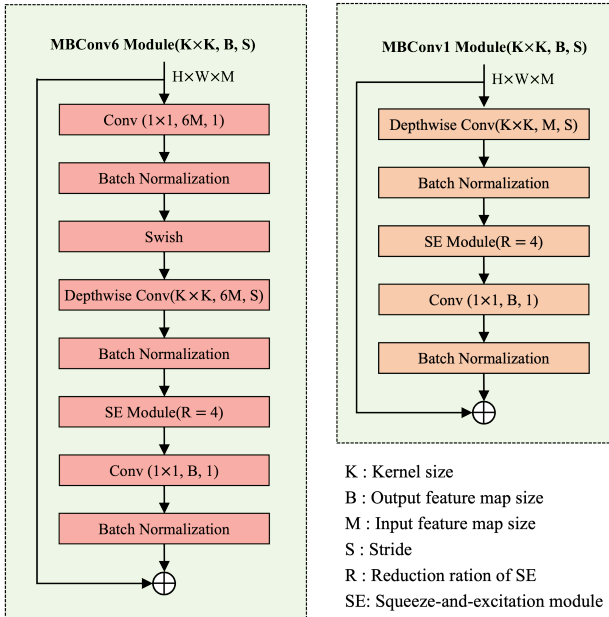


Figure 3: The architecture module of MBConv1 and MBConv6

2.2. The FAGC module

According to shape space theory, the vertices of the shape structure are usually required to be two or three dimensional. Therefore, the Cu-Cr-Zr image features obtained from the EfficientNet-B6 network need to be up-dimensioned to twice their original number before being projected into the Pre-shape space. The up-dimensioned can be achieved by adding techniques such as interpolation or transformation. Here, we replicate a feature as two identical features. Suppose a Cu-Cr-Zr image feature is $V_0 =$

$\{x_1, x_2, \dots, x_n\}$, where n denotes the dimension of the feature. The up-dimensioned function is predefined as $f(x) = x$, i.e., transforming V_0 to $V_1 = \{x_1, y_1, x_2, y_2, \dots, x_n, y_n | y_i = x_i, i \in [1, n]\}$. To remove the influence of feature vector position, the mean of the feature is removed, and the new feature $V_2 = \{x'_1, y'_1, x'_2, y'_2, \dots, x'_n, y'_n | x'_i = x_i - X_\mu, y'_i = y_i - Y_\mu, i \in [1, n]\}$, where X_μ, Y_μ are the mean values of $\{x_i\}$ and $\{y_i\}$, respectively. Then, the scaling of the feature V_2 is excluded with formula $z = V_2 / \|V_2\|$, where $\|V_2\|$ denotes the Euclidean norm of V_2 . Thus, a Cu-Cr-Zr image features are projected into the Pre-shape space as a vector, and the above process is shown in Figure 4. Then, the FAGC method can be employed for feature augmentation [33].

In the Pre-shape space, the Geodesic distance is a crucial metric for describing similarity between two vectors. Suppose z^1 and z^2 denote two vectors in the Pre-shape space, and the Geodesic distance between them is defined by [34, 35]:

$$d(z^1, z^2) = \cos^{-1}(\langle z^1, z^2 \rangle), \quad (2)$$

where $\langle z^1, z^2 \rangle$ denotes the inner product between z^1 and z^2 . Then, the Geodesic curve between z^1 and z^2 can be derived as follows [29]:

$$\Gamma_{(z^1, z^2)}(s) = (\cos s) \cdot z^1 + (\sin s) \frac{z^2 - z^1 \cdot \cos \theta_{(z^1, z^2)}}{\sin \theta_{(z^1, z^2)}}, \quad (3)$$

$$(0 \leq s \leq \theta_{(z^1, z^2)})$$

where $\theta_{(z^1, z^2)}$ denotes the Geodesic distance between z^1 and z^2 , and s is the angle that denotes the Geodesic distance from the new vector z to z^1 .

If more than two images are projected into a Pre-shape space, an optimal Geodesic curve can be constructed with the FAGC method. If the set of feature vectors is denoted as $Z = \{z^1, z^2, \dots, z^M\}$, where M represents the number of

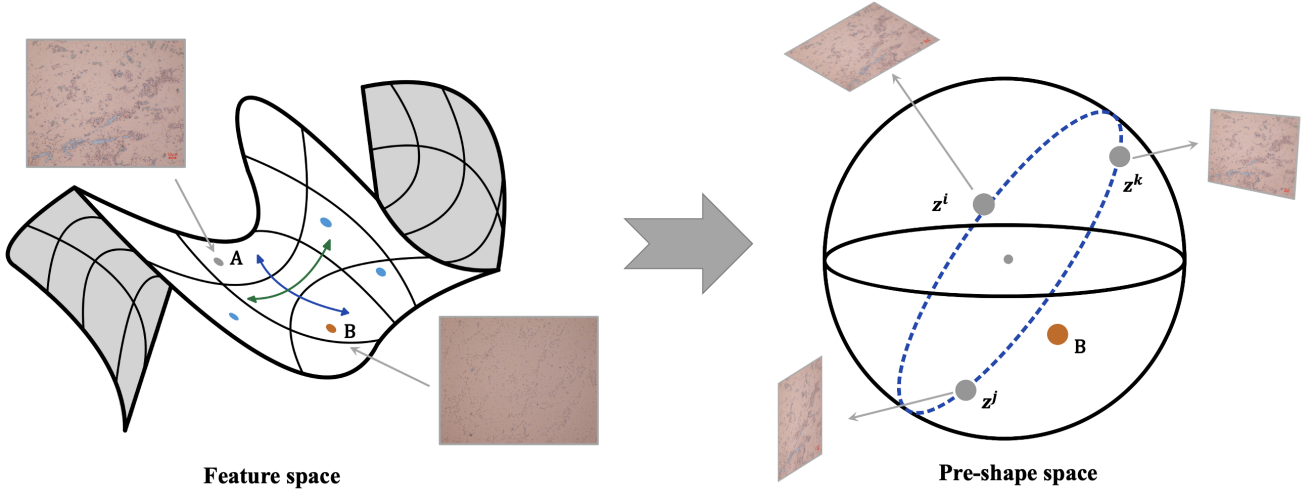


Figure 4: The projection process of Cu-Cr-Zr images from feature space to Pre-shape space. A and B represent two Cu-Cr-Zr images in the feature space. The blue dashed describes the feature vectors from image A, where the vectors z^i, z^j, z^k represent three configurations of A.

features, then the sum of the Geodesic distances between any two vectors can be calculated. The vector corresponding to the maximum cumulative distance is identified as v^* , i.e.,

$$v^* = \operatorname{argmax}_{z^i} \sum_{j=1}^M d(z^i, z^j), i \in \{1, \dots, M\} \quad (4)$$

where $d(z^i, z^j)$ denotes the Geodesic distance between z^i and z^j , calculated by the formula (2). Two feature vectors furthest from v^* are denoted as w^0 and w^1 , respectively. Then, a set of feature vectors on the Geodesic curve $\Gamma_{(w^0, w^1)}(\cdot)$ is calculated, denoted as $\hat{w}^{\{1, \dots, S\}} = \{\Gamma_{(w^0, w^1)}(s^1), \Gamma_{(w^0, w^1)}(s^2), \dots, \Gamma_{(w^0, w^1)}(s^S)\}$. Thus, multiple Geodesic curves between v^* and $\hat{w}^{\{1, \dots, S\}}$ are constructed, denoted as $\Gamma_{(v^*, \hat{w}^{\{1, \dots, S\}})}(\cdot)$. Furthermore, the sum of squared Geodesic distances from the feature set Z to the set of Geodesic curves $\Gamma_{(v^*, \hat{w}^{\{1, \dots, S\}})}(\cdot)$ is computed, and the feature vector w^* which is corresponding to the minimum sum of squared Geodesic distance is calculated as follows:

$$\hat{w}^* = \operatorname{argmin}_{\hat{w}^k} \sum_{j=1}^M \left(d(z^j, \Gamma_{(v^*, \hat{w}^k)}(\cdot)) \right)^2, i \in \{1, \dots, S\} \quad (5)$$

\hat{w}^* is assigned to v^* , and the above steps are repeated iteratively until \hat{w}^* and v^* cease to change, denoting \hat{w}^* as w^* . Thus, $\Gamma_{(v^*, w^*)}$ is the optimal Geodesic curve fitting the distribution of the feature vector set Z .

Then, a series of generated features are constructed along the Geodesic curve $\Gamma_{(v^*, w^*)}(\cdot)$. Meanwhile, to enrich the diversity of the features, a uniform distribution $s \sim U(0, d(v^*, w^*))$ is employed to sample a set of values $\{s^1, s^2, \dots, s^K\}$, where K denotes the number of angles and also the number of generated features. Then, a series of feature vectors is obtained by substituting these values into the Geodesic curve function $\Gamma_{(v^*, w^*)}(\cdot)$, denoted as $G = \{g^1, g^2, \dots, g^K\}$.

2.3. The design of pseudo-labeling

To fully exploit the information within the generated features, a pseudo-labeling mechanism is designed. The high performance network EfficientNet-B6 is initially chosen as the regression model, denoted R_a . The performance of the generated feature set G is predicted, yielding a set of predicted results $\{p_1, p_2, \dots, p_K\} = R_a(G)$, where $\{p_1, p_2, \dots, p_K\}$ are the corresponding predicted performance values. These predicted values $\{p_1, p_2, \dots, p_K\}$ are pseudo-labels for the generated feature set G .

Thus, a new and more enriched feature dataset can be created by expanding the original feature set. The created dataset is a combination of the original image feature set Z and the generated feature set G with pseudo-labels, denoted as $Z' = \{z^1, \dots, z^M, g^1, \dots, g^K\}$, where M and K are numbers of the original and generated feature sets, respectively. Subsequently, other machine learning models are employed to train the expanded feature set Z' . The training objective of the model is to minimize the mean squared error of the model until the error converges to stability. To optimize predictions for each element in the feature set Z' , and the optimal regression model R_b is obtained, which can predict the electrical conductivity and the hardness properties of Cu-Cr-Zr more accurately. Figure (5) comprehensively illustrates the sequence of steps from selecting the generated feature set to training the ultimate regression model.

3. Results

3.1. Dataset and EfficientNet model

The Cu-Cr-Zr image dataset contains 18 images as shown in Figure 6. The number of images for the Cu-Cr-Zr material is too small and poses a challenge for dealing. Figure 7 describe the distribution of electrical conductivity and hardness of the Cu-Cr-Zr material, respectively. As

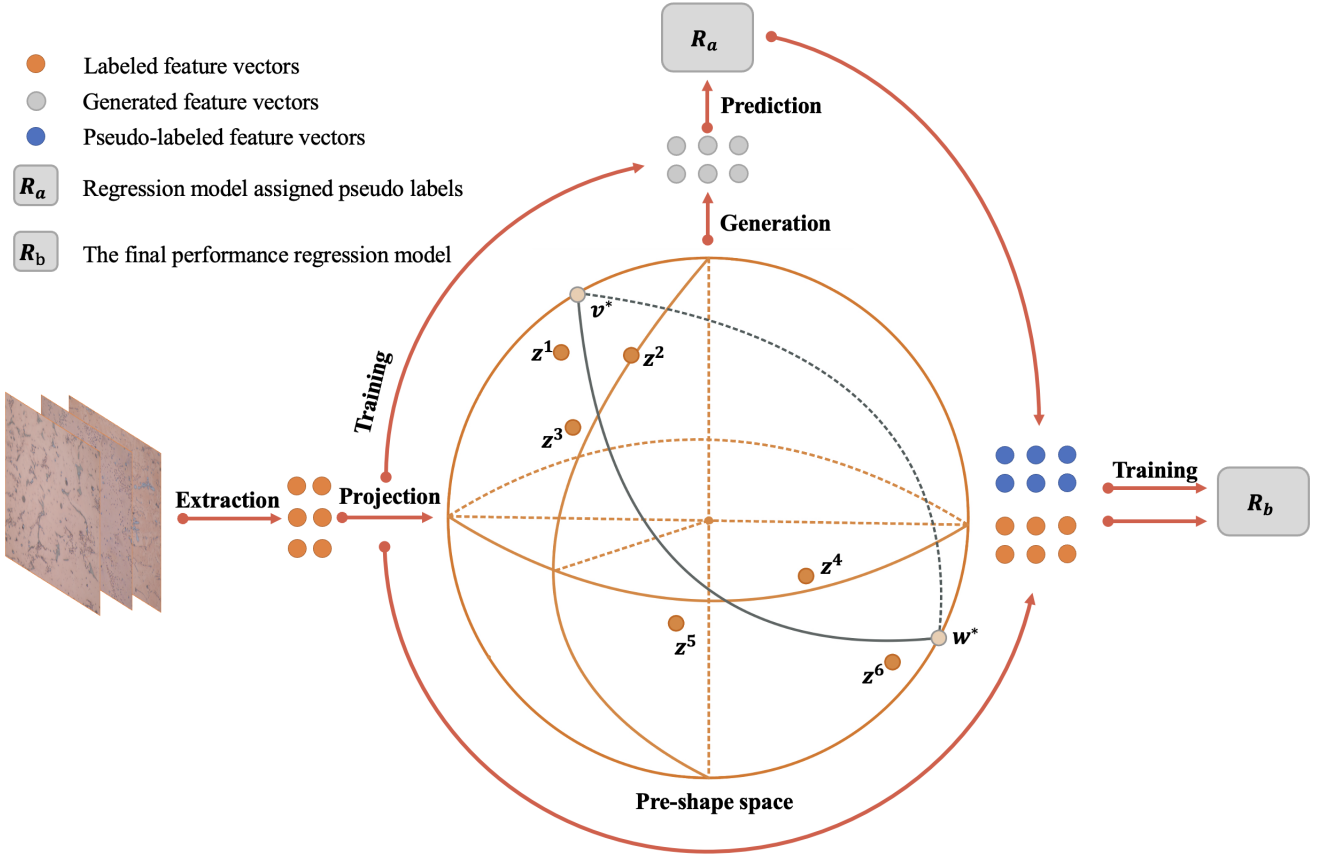


Figure 5: The workflow for feature augmentation on the Geodesic curve with regression models.

above mentioned, to determine the optimal EfficientNet model, including EfficientNet-B0~EfficientNet-B7 are trained. Here, the standard model performance metrics such as R^2 -score, MAE, MSE, and RMSE are employed for performance evaluation. The R^2 reflects the degree of fit between the predicted values of the model and the actual observations. It is commonly used to compare the predictive ability of different models. The MAE (mean absolute error) is utilized to quantify the average absolute differences between predicted values and the actual observed values. The MSE (mean square error) and the RMSE (root mean square error) used as the indicators to describe the extent of deviation between predicted values and actual observations. The advantage of the RMSE is that it incorporates squared terms, thereby reducing the influence of outliers on model evaluation. Suppose the predicted values of the model are $\{y_{pred}^1, y_{pred}^2, \dots, y_{pred}^N\}$, and the actual observations are $\{y_{true}^1, y_{true}^2, \dots, y_{true}^N\}$, where N is the number of image samples, then the metrics are calculated as follows:

$$R^2 = 1 - \frac{\sum_{i=1}^N (y_{true}^i - y_{pred}^i)^2}{\sum_{i=1}^N (y_{true}^i - \bar{y}_{true})^2}, \quad (6)$$

and

$$MAE = \frac{1}{N} \sum_{i=1}^N |y_{true}^i - y_{pred}^i|, \quad (7)$$

and

$$RMSE = \sqrt{\frac{1}{N} \sum_{i=1}^N (y_{true}^i - y_{pred}^i)^2}, \quad (8)$$

where \bar{y}_{true} denotes the average value of all observations. The value of R^2 takes on the range of $(-\infty, 1]$. The closer is to 1, the better the generalization ability of the model. The values of MAE and RMSE take the range of $[0, +\infty)$. The closer the MAE value is to 0, the smaller the average prediction error of the model. The closer the RMSE value is to 0, the better the predictive performance of the model.

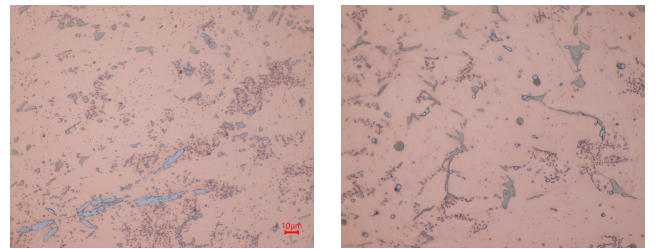


Figure 6: Image sample example diagram of Cu-Cr-Zr.

In addition, a 6-fold cross-validation method is employed to partition the dataset. In each iteration, a fold consist 3 test images and 15 train images. The model is pre-trained

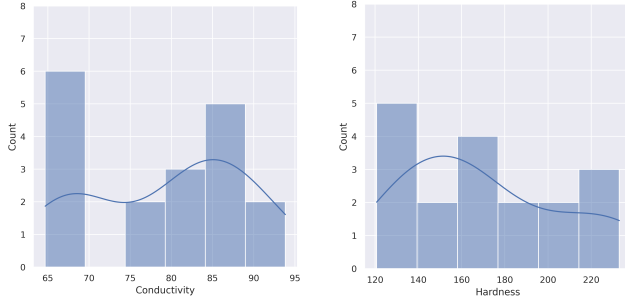


Figure 7: Distribution of electrical conductivity and hardness performance in Cu-Cr-Zr. "Count" means the number of samples in the specified performance.

Table 1

Comparative analysis of different EfficientNet(ENet) architectures for predicting conductivity and hardness in Cu-Cr-Zr alloy images. R^2 quantifies the generalization ability of the model. MAE quantifies the average absolute differences between predicted values and the actual observed values. RMSE represents the extent of deviation between predicted values and actual observations.

Network	Conductivity			Hardness		
	R^2	MAE	RMSE	R^2	MAE	RMSE
ENet-B0	0.326	9.674	10.348	0.389	32.532	35.428
ENet-B1	0.334	9.452	10.287	0.427	31.975	34.317
ENet-B2	0.487	8.375	9.031	0.496	29.863	32.191
ENet-B3	0.559	8.164	8.376	0.559	28.613	30.079
ENet-B4	0.556	7.963	8.395	0.553	27.462	30.291
ENet-B5	0.570	7.682	8.263	0.557	27.521	30.172
ENet-B6	0.606	7.415	7.918	0.619	26.883	27.981
ENet-B7	0.591	6.872	8.061	0.598	28.947	28.763

with ImageNet data to initialize the network weights. The loss function is selected as the mean square error, and the optimizer is chosen as Adam[36] with an initial learning rate of 0.0001. An adaptive learning rate decay strategy is used with a total training epoch of 200. The experimental results are shown in Table 1. Thus, the selection of the EfficientNet-B6 model is chosen as the optimal feature extraction model based on the performance metrics results.

3.2. The performance prediction of Cu-Cr-Zr

To comprehensively evaluate the augmentation influence of with the FAGC module on the regression model. Two sets of experiments are completed to predict the conductivity performance and hardness of Cu-Cr-Zr. The sets of the machine learning methods include Linear Regression(LR), KNN Regressor(KNN)[37], AdaBoost[38], ExtraTree[39], DecisionTree[5], and Bagging[40] which are original or combined with the FAGC module.

Figure 8 illustrates the performance prediction results for Cu-Cr-Zr conductivity. The red dashed line represents a perfect correlation between the actual and the predicted value. Each blue point forms a two-dimensional coordinate pair representing the predicted and actual values. If the blue point is closer to the red dashed line, the predicted

Table 2

Performance prediction of electrical conductivity in Cu-Cr-Zr using the EfficientNet-B6(ENet-B6) network with FAGC.

Regressor	R^2	MAE	RMSE
LR	0.548	8.136	8.476
KNN [37]	0.605	7.423	7.915
AdaBoost[38]	0.663	6.957	7.319
ExtraTree[39]	0.763	4.910	6.132
DecisionTree[5]	0.609	7.192	7.883
Bagging[40]	0.689	6.829	7.026
ENet-B6	0.606	7.415	7.918
ENet-B6 + LR + FAGC	0.510	8.740	8.825
ENet-B6 + KNN + FAGC	0.660	7.021	7.352
ENet-B6 + AdaBoost + FAGC	0.710	6.505	6.785
ENet-B6 + ExtraTree + FAGC	0.879	4.134	4.378
ENet-B6 + DecisionTree + FAGC	0.978	1.632	1.882
ENet-B6 + Bagging + FAGC	0.756	6.202	6.227

Table 3

Performance prediction of hardness in Cu-Cr-Zr using the EfficientNet-B6(ENet-B6) network with FAGC.

Regressor	R^2	MAE	RMSE
LR	0.483	28.632	32.558
KNN [37]	0.539	26.891	30.785
AdaBoost[38]	0.504	23.207	31.918
ExtraTree[39]	0.550	18.118	30.416
DecisionTree[5]	0.638	19.675	27.272
Bagging[40]	0.430	24.971	34.226
ENet-B6	0.604	26.883	28.549
ENet-B6 + LR + FAGC	0.477	28.779	32.780
ENet-B6 + KNN + FAGC	0.557	25.970	30.193
ENet-B6 + AdaBoost + FAGC	0.915	11.057	13.219
ENet-B6 + ExtraTree + FAGC	0.968	5.632	8.071
ENet-B6 + DecisionTree + FAGC	0.998	1.598	1.997
ENet-B6 + Bagging + FAGC	0.670	19.188	26.035

performance value is closer to the actual Cu-Cr-Zr conductivity performance. The experimental results demonstrate the significant influence of the FAGC module in improving the prediction performance of the regression model. The regression performance of machine learning models significantly outperforms the benchmarks after incorporating the FAGC module. Especially for the DecisionTree model, the R^2 , MAE and RMSE reach 0.978 and 1.882, respectively. In addition, the experimental results illustrate the generalization and effectiveness of the FAGC module in different regression models. The detailed experimental results are shown in Table 2.

For the hardness performance prediction of Cu-Cr-Zr, a range of machine learning regression models is employed for comparison against the FAGC module, adhering to the experimental approaches detailed in section 3.1. Table 3 provides an overview of the performance metrics associated with various regression models predicting hardness. The

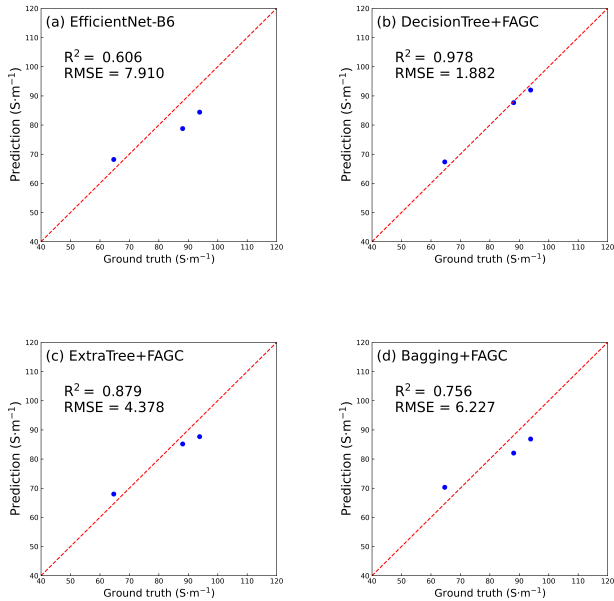


Figure 8: Comparison of the prediction and observation of electrical conductivity in Cu-Cr-Zr with FAGC across different regression models.

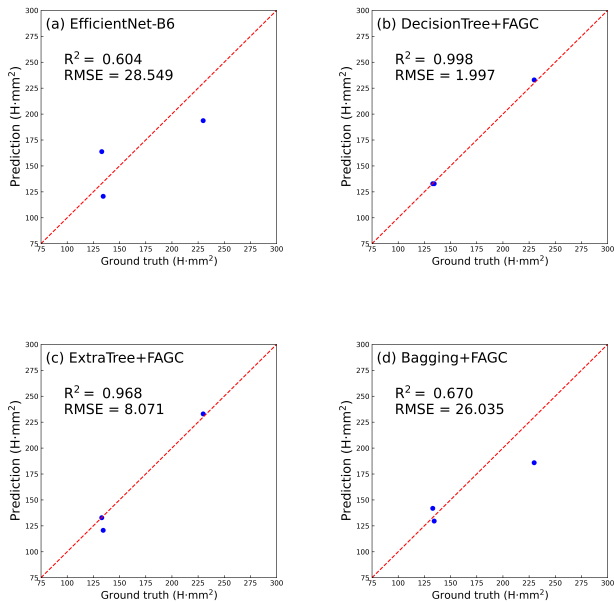


Figure 9: Comparison of the prediction and observation of hardness in Cu-Cr-Zr with FAGC across different regression models.

DecisionTree model notably outperforms others in predicting hardness. Figure 9 illustrates a comparative analysis of the prediction results. For the hardness prediction of Cu-Cr-Zr, the EfficientNet-B6 network reaches an R^2 of 0.604, an MAE of 26.883, an MSE of 815.018, and an RMSE of 28.549. However, most machine learning regression models perform below the EfficientNet-B6 benchmark. In contrast,

the introduction of the FAGC module significantly improves the predictive accuracy of these regression models across all metrics. The improved prediction accuracy is attributed to the effectiveness of the Geodesic curve in fitting its feature distribution region, even with a limited set of feature data. The effective utilization of feature data from Geodesic curves and the expansion of the dataset are achieved through the pseudo-labeling mechanism, which contributes to the enrichment of the dataset diversity. Especially for the DecisionTree and ExtraTree models, the R^2 reach 0.998 and 0.968, respectively. The experimental results once again validate the outstanding effectiveness and versatility of the FAGC module in predicting the hardness performance of Cu-Cr-Zr.

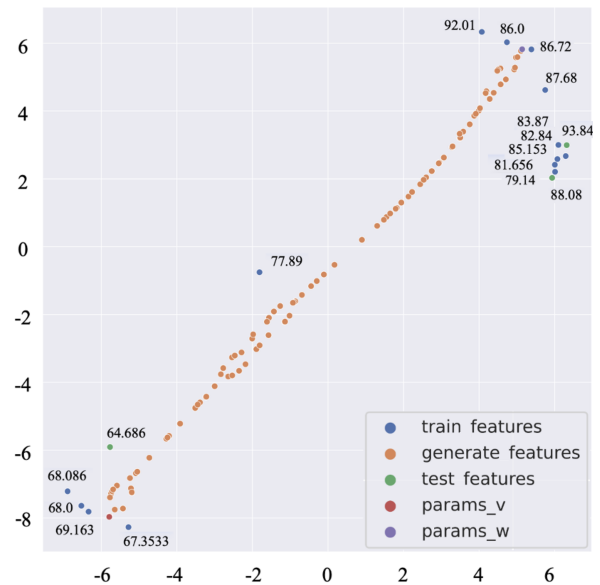


Figure 10: Visualization of the generated features and actual features of the Cu-Cr-Zr material through t-SNE. The blue points represent the features of the Cu-Cr-Zr training set images; the green points correspond to the features of the Cu-Cr-Zr test set; the orange points indicate the generated features; the red and purple points denote the optimal parameters v^* and w^* of the Geodesic curve, respectively.

3.3. Exploring performance relationships between generated and Cu-Cr-Zr features via t-SNE visualization

To investigate the correlation between the generated features and actual features of the Cu-Cr-Zr material, we use the t-SNE (t-distributed stochastic neighbor embedding) method to downscale the feature data for visualization. By mapping the feature data into a two-dimensional space, we observe the distribution between the generated features and actual features of the Cu-Cr-Zr material as shown in Figure 10. In Figure 10, the training and test features of Cu-Cr-Zr are represented by blue and green dots, respectively. The orange dots represent the generated features, while the red and purple dots represent the two endpoints of the optimal Geodesic curve. The Geodesic curve can fit the feature

region of Cu-Cr-Zr, and the effectiveness of the FAGC module is verified. The conductivity property values of Cu-Cr-Zr are labeled in the figure. The characteristics of Cu-Cr-Zr are mainly distributed in the lower left and upper right regions, which its conductivity performance value increases trend from the lower left to the upper right. It is worth noting that the trend of conductivity performance is closely related to the distribution region of the generated features, indicating that assigning pseudo-labels to generated features is reasonable and effective.

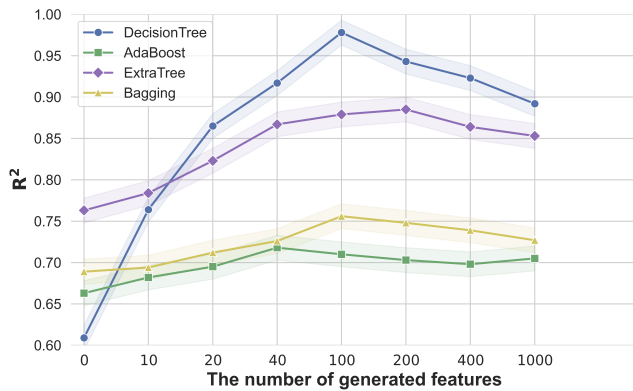


Figure 11: The R^2 of the different numbers of the generated feature vectors in Cu-Cr-Zr conductivity prediction.

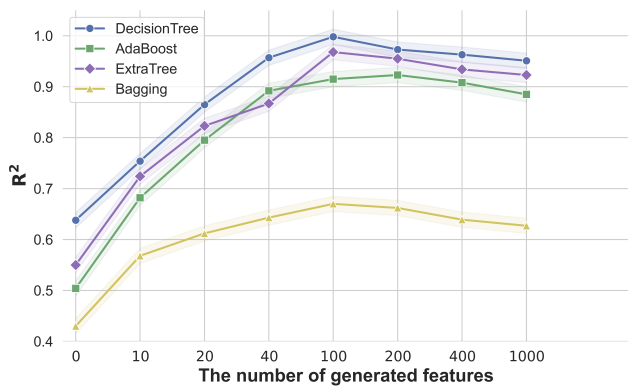


Figure 12: The R^2 of the different numbers of the generated feature vectors in Cu-Cr-Zr hardness prediction.

3.4. The influence of the number of generated features on performance prediction of Cu-Cr-Zr

An experiment is conducted to evaluate the influence of the number of features generated from the FAGC module. Several machine learning regression models are used to predict the performance of Cu-Cr-Zr conductivity and hardness, including AdaBoost, ExtraTree, DecisionTree, and Bagging. The feature extraction model is employed EfficientNet-B6, with the number of generated features including 10, 20, 40, 100, 200, 400, and 1000. The experimental results are presented in Figure 11 and Figure 12. The experimental

results indicate that increasing the number of features generated can significantly improve the predictive ability of the model. However, the number of generated features and R^2 of the regression model is not strictly monotonous. Excessive generated features can cause the model to focus too much on the distribution of generated features, neglecting the distribution of authentic features. Therefore, the performance of the model does not grow in proportion to the size of the generated features. In our Cu-Cr-Zr dataset, about 100 features is generated to obtain the optimal results, which is about five times the size of the original dataset. Under these conditions, most models demonstrate superior predictive performance.

3.5. The influence of pseudo-label quality on the model

In order to evaluate the influence of pseudo-label quality on the performance of the regression models, a set of experiments which predict the electrical conductivity and hardness of Cu-Cr-Zr show the qualities of pseudo-labels generated with DecisionTree, AdaBoost, ExtraTree, or Bagging. These methods for generating pseudo-labels are described as R_a in Figure 13 and Figure 14. The results of the comparative experiments are illustrated in Figure 13 and Figure 14, and the applied regression model training strategy aligns with the description in section 3.1. The experimental results show that the quality of the pseudo-labels has a significant influence on the performance of the regression model. The DecisionTree model reveals the optimal performance in the R^2 and the RMSE.

4. Conclusion

In our study, we introduce an advanced method to predict the conductivity and hardness of Cu-Cr-Zr alloys based on their microstructures, employing a technique referred to as FAGC (Feature Augmentation on Geodesic Curves). This approach is structured in two primary stages to improve performance prediction accuracy: Initially, we extract features from images of Cu-Cr-Zr alloys using the EfficientNet-B6 neural network architecture. This step is crucial for capturing the intricate details within the alloy's microstructure that influence its properties. Subsequently, these extracted image features are mapped onto a mathematical framework known as Pre-shape space. Here, the FAGC module plays a pivotal role in refining the feature data and generating additional, informative feature data.

Our methodology is rigorously compared against several machine learning models, revealing that the incorporation of the FAGC module significantly boosts the R^2 values of the regression models used in our predictions. Notably, the decision tree model, after integrating the FAGC module, achieved impressive R^2 scores of 0.978 and 0.998. These results not only highlight the improved predictive accuracy and generalization capability of our method under constrained data scenarios but also pave the way for addressing complex predictive challenges in materials similar to Cu-Cr-Zr alloys.

Revealing the structure-property relationships of copper alloys with FAGC

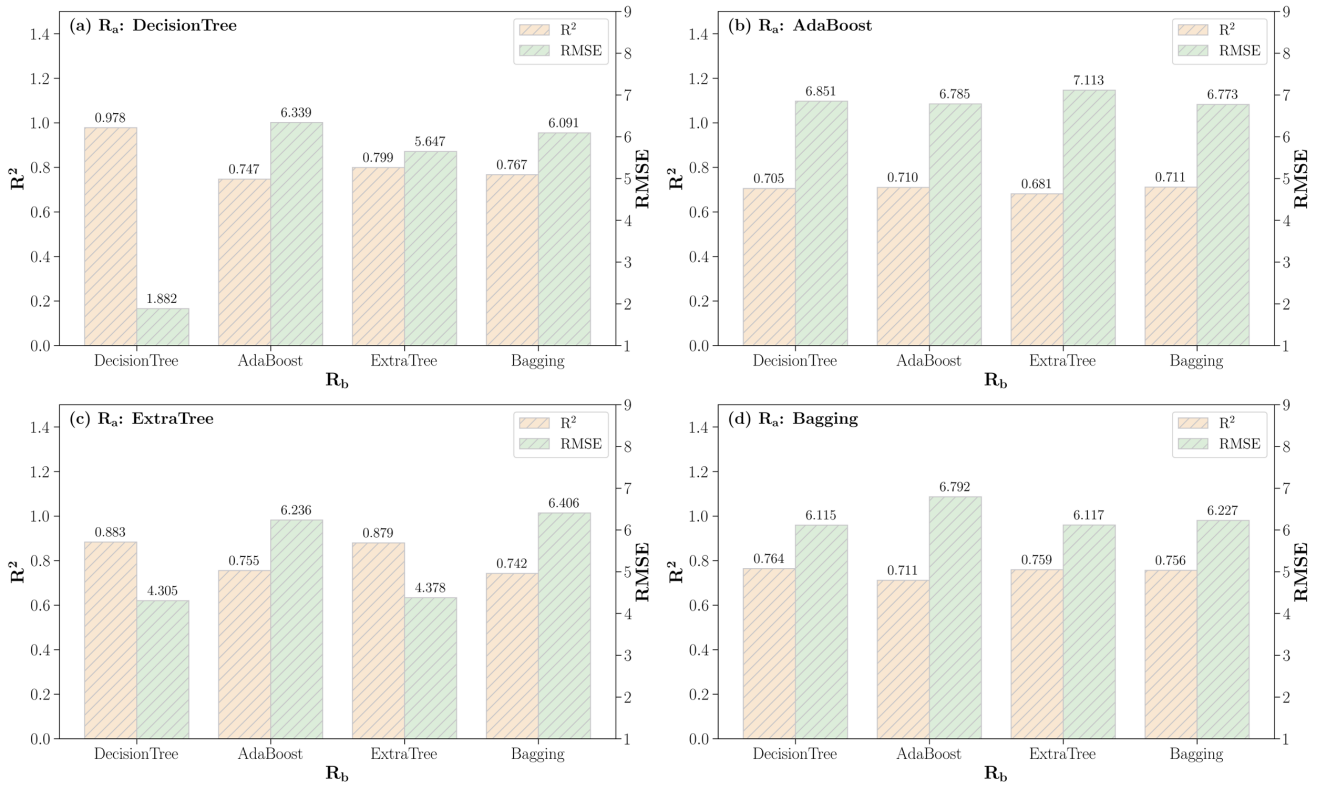


Figure 13: The influence of pseudo-label quality on regression models in Cu-Cr-Zr conductivity prediction. R_a means the regression model for predicting pseudo-labeling. R_b represents the final regression model.

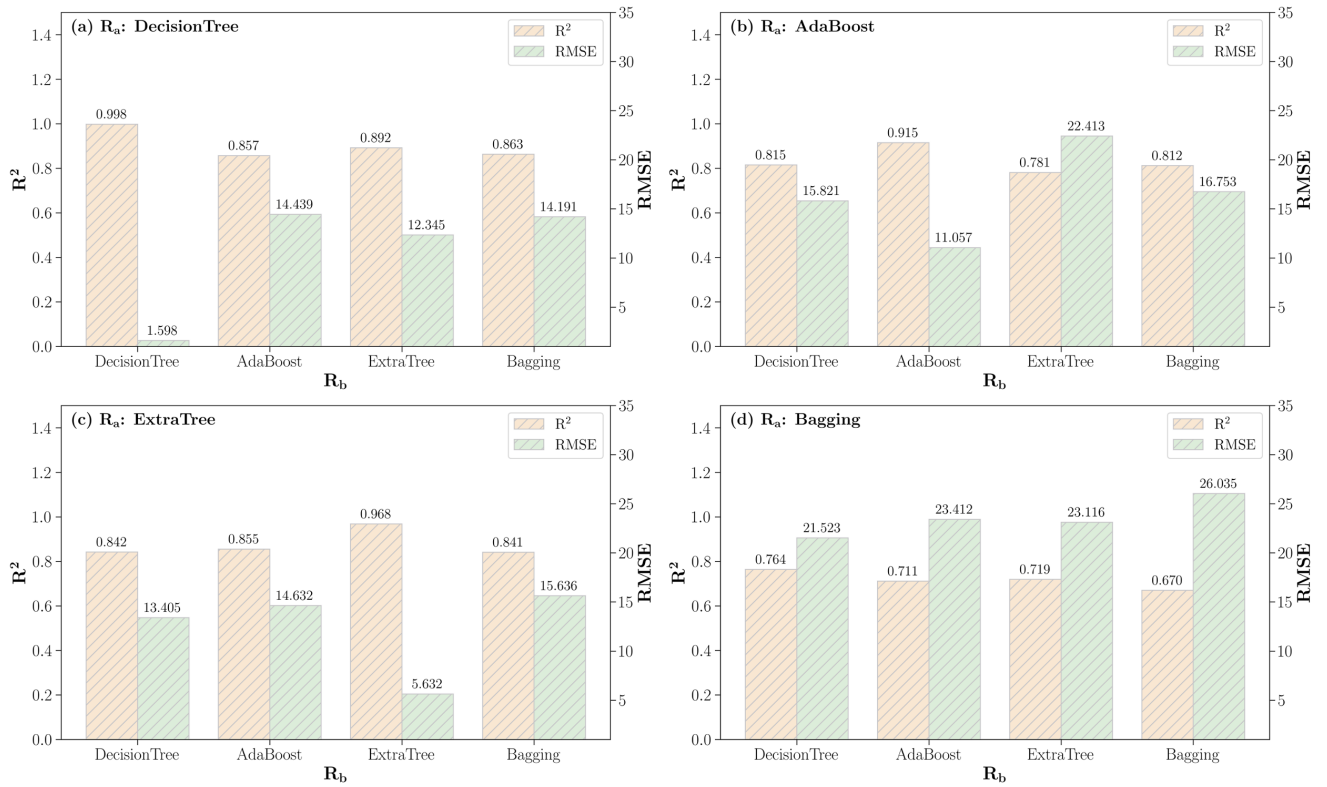


Figure 14: The influence of pseudo-label quality on regression models in Cu-Cr-Zr hardness prediction. R_a means the regression model for predicting pseudo-labeling. R_b represents the final regression model.

Furthermore, this study demonstrates the synergistic integration of machine learning and shape space theory, offering deeper insights into the properties of Cu-Cr-Zr alloys. It proves to be a robust approach for machine learning applications, especially when faced with limited sample data. Our research contributes both theoretical and practical advancements that are of significant benefit to both academia and the industry, providing a solid foundation for the prediction of material properties.

5. Acknowledgement

This research is sponsored by National Natural Science Foundation of China (Grant No. 52273228, 52373227), Key Program of Science and Technology of Yunnan Province (202302AB080022), the Project of Key Laboratory of Silicate Cultural Relics Conservation (Shanghai University), Ministry of Education (No. SCRC2023ZZ07TS).

References

- [1] Rampi Ramprasad, Rohit Batra, Ghanshyam Pilania, Arun Mannodi-Kanakthodi, and Chiho Kim. Machine learning in materials informatics: recent applications and prospects. *npj Computational Materials*, 3(1):54, 2017.
- [2] Vladimir Vapnik. Support-vector networks. *Machine learning*, 20:273–297, 1995.
- [3] Thorsten Joachims. Text categorization with support vector machines: Learning with many relevant features. In *European conference on machine learning*, pages 137–142. Springer, 1998.
- [4] Harris Drucker, Christopher J Burges, Linda Kaufman, Alex Smola, and Vladimir Vapnik. Support vector regression machines. *Advances in neural information processing systems*, 9, 1996.
- [5] Leo Breiman. *Classification and regression trees*. Routledge, 2017.
- [6] Ruoqian Liu, Yuksel C Yabansu, Ankit Agrawal, Surya R Kalidindi, and Alok N Choudhary. Machine learning approaches for elastic localization linkages in high-contrast composite materials. *Integrating Materials and Manufacturing Innovation*, 4:192–208, 2015.
- [7] Zhixiong Li, Dazhong Wu, and Tianyu Yu. Prediction of material removal rate for chemical mechanical planarization using decision tree-based ensemble learning. *Journal of Manufacturing Science and Engineering*, 141(3):031003, 2019.
- [8] Alex Krizhevsky, Ilya Sutskever, and Geoffrey E Hinton. Imagenet classification with deep convolutional neural networks. *Advances in neural information processing systems*, 25, 2012.
- [9] Matthew D Zeiler and Rob Fergus. Visualizing and understanding convolutional networks. In *Computer Vision—ECCV 2014: 13th European Conference, Zurich, Switzerland, September 6–12, 2014, Proceedings, Part I 13*, pages 818–833. Springer, 2014.
- [10] Karen Simonyan and Andrew Zisserman. Very deep convolutional networks for large-scale image recognition. *arXiv preprint arXiv:1409.1556*, 2014.
- [11] Yann LeCun, Léon Bottou, Yoshua Bengio, and Patrick Haffner. Gradient-based learning applied to document recognition. *Proceedings of the IEEE*, 86(11):2278–2324, 1998.
- [12] Olga Russakovsky, Jia Deng, Hao Su, Jonathan Krause, Sanjeev Satheesh, Sean Ma, Zhiheng Huang, Andrej Karpathy, Aditya Khosla, Michael Bernstein, et al. Imagenet large scale visual recognition challenge. *International journal of computer vision*, 115:211–252, 2015.
- [13] Kaiming He, Xiangyu Zhang, Shaoqing Ren, and Jian Sun. Deep residual learning for image recognition. In *Proceedings of the IEEE conference on computer vision and pattern recognition*, pages 770–778, 2016.
- [14] Mingxing Tan and Quoc Le. Efficientnet: Rethinking model scaling for convolutional neural networks. In *International conference on machine learning*, pages 6105–6114. PMLR, 2019.
- [15] Yuexing Han, Ruting Chi, Qiaochuan Chen, Bing Wang, Wei Liu, and Yanlin He. Microstructural evolution and coarsening behavior of the precipitates in 2205 duplex stainless steel aged at 850° c. *Journal of Materials Research and Technology*, 26:2560–2574, 2023.
- [16] Chengjie Du, Guisheng Zou, A Zhanwen, Bingzhou Lu, Bin Feng, Jinpeng Huo, Yu Xiao, Yang Jiang, and Lei Liu. Highly accurate and efficient prediction of effective thermal conductivity of sintered silver based on deep learning method. *International Journal of Heat and Mass Transfer*, 201:123654, 2023.
- [17] Han Wei, Shuaishuai Zhao, Qingyuan Rong, and Hua Bao. Predicting the effective thermal conductivities of composite materials and porous media by machine learning methods. *International Journal of Heat and Mass Transfer*, 127:908–916, 2018.
- [18] Moran Wang, Jinku Wang, Ning Pan, and Shiyi Chen. Mesoscopic predictions of the effective thermal conductivity for microscale random porous media. *Physical Review E*, 75(3):036702, 2007.
- [19] Connor Shorten and Taghi M Khoshgoftaar. A survey on image data augmentation for deep learning. *Journal of big data*, 6(1):1–48, 2019.
- [20] Ian Goodfellow, Jean Pouget-Abadie, Mehdi Mirza, Bing Xu, David Warde-Farley, Sherjil Ozair, Aaron Courville, and Yoshua Bengio. Generative adversarial nets. *Advances in neural information processing systems*, 27, 2014.
- [21] Diederik P Kingma and Max Welling. Auto-encoding variational bayes. *arXiv preprint arXiv:1312.6114*, 2013.
- [22] Pan Li, Da Li, Wei Li, Shaogang Gong, Yanwei Fu, and Timothy M Hospedales. A simple feature augmentation for domain generalization. In *Proceedings of the IEEE/CVF International Conference on Computer Vision*, pages 8886–8895, 2021.
- [23] Boyi Li, Felix Wu, Ser-Nam Lim, Serge Belongie, and Kilian Q Weinberger. On feature normalization and data augmentation. In *Proceedings of the IEEE/CVF conference on computer vision and pattern recognition*, pages 12383–12392, 2021.
- [24] David G Kendall. Shape manifolds, procrustean metrics, and complex projective spaces. *Bulletin of the London mathematical society*, 16(2):81–121, 1984.
- [25] Yuexing Han. Recognize objects with three kinds of information in landmarks. *Pattern Recognition*, 46(11):2860–2873, 2013.
- [26] Yuexing Han, Hideki Koike, and Masanori Idesawa. Recognizing objects with multiple configurations. *Pattern Analysis and Applications*, 17:195–209, 2014.
- [27] Kim Evans. Curve-fitting in shape space. *Quantitative biology, shape analysis, and wavelets*. Leeds University Press, Leeds, 2005.
- [28] Kim Kenobi, Ian L Dryden, and Huiling Le. Shape curves and geodesic modelling. *Biometrika*, 97(3):567–584, 2010.
- [29] Yuexing Han, Bing Wang, Masanori Idesawa, and Hiroyuki Shimai. Recognition of multiple configurations of objects with limited data. *Pattern Recognition*, 43(4):1467–1475, 2010.
- [30] Mark Sandler, Andrew Howard, Menglong Zhu, Andrey Zhmoginov, and Liang-Chieh Chen. Mobilenetv2: Inverted residuals and linear bottlenecks. In *Proceedings of the IEEE conference on computer vision and pattern recognition*, pages 4510–4520, 2018.
- [31] François Chollet. Xception: Deep learning with depthwise separable convolutions. In *Proceedings of the IEEE conference on computer vision and pattern recognition*, pages 1251–1258, 2017.
- [32] Prajit Ramachandran, Barret Zoph, and Quoc V Le. Searching for activation functions. *arXiv preprint arXiv:1710.05941*, 2017.
- [33] Yuexing Han, Guanxin Wan, and Bing Wang. Fagc:feature augmentation on geodesic curve in the pre-shape space, 2023.
- [34] IL Dryden and KV Mardia. *Statistical shape analysis*.(wiley: New york, ny.). 1998.
- [35] Christopher G Small. *The statistical theory of shape*. Springer Science & Business Media, 2012.
- [36] Diederik P Kingma and Jimmy Ba. Adam: A method for stochastic optimization. *arXiv preprint arXiv:1412.6980*, 2014.

- [37] Thomas Cover and Peter Hart. Nearest neighbor pattern classification. *IEEE transactions on information theory*, 13(1):21–27, 1967.
- [38] Yoav Freund, Robert E Schapire, et al. Experiments with a new boosting algorithm. In *icml*, volume 96, pages 148–156. Citeseer, 1996.
- [39] Pierre Geurts, Damien Ernst, and Louis Wehenkel. Extremely randomized trees. *Machine learning*, 63:3–42, 2006.
- [40] Leo Breiman. Bagging predictors. *Machine learning*, 24:123–140, 1996.